iPTF14hls: A unique long-lived supernova from a rare explosion channel

I. Arcavi[1,2], et al.

[1] *Las Cumbres Observatory Global Telescope Network, Santa Barbara, CA 93117, USA.*

[2] *Kavli Institute for Theoretical Physics, University of California, Santa Barbara, CA 93106, USA.*

Most hydrogen-rich massive stars end their lives in catastrophic explosions known as Type IIP supernovae, which maintain a roughly constant luminosity for $\approx$100 days and then decline. This behavior is well explained as emission from a shocked and expanding hydrogen-rich red supergiant envelope, powered at late times by the decay of radioactive ^{56}Ni produced in the explosion[1,2,3]. As the ejected mass expands and cools it becomes transparent from the outside inwards, and decreasing expansion velocities are observed as the inner slower-moving material is revealed. Here we present iPTF14hls, a nearby supernova with spectral features identical to those of Type IIP events, but remaining luminous for over 600 days with at least five distinct peaks in its light curve and expansion velocities that remain nearly constant in time. Unlike other long-lived supernovae, iPTF14hls shows no signs of interaction with circumstellar material. Such behavior has never been seen before for any type of supernova and it challenges all existing explosion models. Some of the properties of iPTF14hls can be explained by the formation of a long-lived central power source such as the spindown of a highly magentized neutron star[4,5,6] or fallback accretion onto a black hole[7,8]. The ejection of a massive hydrogen-rich shell in a pulsational pair instability event[9] several years prior

to explosion may explain additional properties of iPTF14hls and points to a progenitor more than 200 times more massive than the sun. If this scenario is correct, it indicates that very massive stars with low metal content (required to retain their hydrogen envelope during most of their evolution) can form in the nearby Universe. If it is not, then a new form of stellar explosion is required to explain iPTF14hls.

On 2014 September 22.53 (UT dates are used throughout), the intermediate Palomar Transient Factory (iPTF)[10, 11] discovered iPTF14hls at right ascension, $\alpha_{\rm J2000} = 09{\rm h}\ 20{\rm min}\ 34.30{\rm s}$ and declination, $\delta_{\rm J2000} = +50°41'46.8''$, at an $R_{\rm PTF}$-band magnitude of 17.716 ± 0.033 (Extended Fig. 1). No source was seen at that position when it was previously visited by iPTF on 2014 May 6.19 down to a 3σ limiting $R_{\rm PTF}$ magnitude of 20.95. iPTF14hls was later independently discovered by the Catalina Real-Time Transient Survey[12] as CSS141118:092034+504148 (more recently the event was reported to the Transient Name Server as AT 2016bse). On 2015 January 8.71, the event was classified as a Type IIP SN at a redshift of $z = 0.028$, based on prominent broad Balmer series P-Cygni lines[13]. Here we adopt a redshift of $z = 0.0344$, determined from narrow host-galaxy features (Extended Fig. 7), corresponding to a luminosity distance of 156.2 Mpc (a standard ΛCDM cosmology[14] is assumed throughout). The host galaxy of iPTF14hls is a star forming dwarf galaxy, with a mass similar to that of the Small Magellanic Cloud (see Methods for details), implying a low metal content[15]. The weak iron-line absorption seen in the SN spectra are also consistent with a low metallicity progenitor (see Methods for details).

In Type IIP events, the SN shock heats and ionizes the ejecta, which later expands, cools and recombines. The photosphere follows the recombination front, which is at a roughly constant temperature ($T_{eff} \approx 6000\,\mathrm{K}$)[1] as it makes its way inwards in mass through the expanding ejecta. This leads to the ≈ 100-day "plateau" (or photospheric) phase of roughly constant luminosity in the light curve and prominent hydrogen P-Cygni features in the spectrum, both of which constitute the observational definition of the Type IIP SN class. Once the recombination front makes it through the hydrogen-rich outer ejecta, the luminosity drops to the radioactive decay tail of ^{56}Co (a product of ^{56}Ni) and nebular emission lines dominate the spectrum. iPTF14hls, in contrast, has yet to become nebular, 600 days after discovery.

Using blackbody fits to the broad-band optical $BVgi$ photometry of iPTF14hls (see Methods for details), we find a roughly constant effective temperature of $5000 - 6000\,\mathrm{K}$, the same as the hydrogen-recombination temperature typically seen in Type IIP SNe. However, the inferred bolometric luminosity of a few$\times 10^{42}\,\mathrm{erg\,s^{-1}}$ is on the high end of what is observed for IIP SNe[16], and the total radiated energy of $2.20^{+0.03}_{-0.05} \times 10^{50}$ erg emitted during the 450 days of our multi-band optical coverage is a factor of a few times larger than any known IIP SN. Due to the gap of 139 days between the last non-detection of iPTF14hls and its discovery, the total luminosity and true duration of iPTF14hls may be even higher.

SNe powered by the interaction of their ejecta with a dense circumstellar material (CSM) can be luminous and long-lived (even out to > 4 years after explosion)[17]. In these cases, however, the interaction dominates the spectra in the form of a strong continuum together with broad, intermediate and narrow components of the Balmer series emission lines[18, 19, 20]. None of these features are seen in the spectra of iPTF14hls (Fig. 2; Extended Fig. 8). We also find no evidence of X-ray or radio emission (which are possible additional indicators of strong interaction) in observations taken during the brightest peak of the optical light curve. We do not detect any signs of polarization indicative of strong asymmetry in the explosion (see Methods for details). Instead, our ≈ 450 day spectral campaign of iPTF14hls, which began on 2015 Feb 11.42, shows that the event remained spectroscopically similar to standard IIP SNe throughout our coverage (Fig. 2), with an evolution approximately 10 times slower compared to that of Type IIP SNe (i.e. the spectrum of iPTF14hls at day 500 looks like that of a IIP SN at day 50, etc; Extended Fig. 3). The slow evolution is intrinsic and not due to time dilation effects (see Methods).

The expansion velocity v of SN ejecta is indicated by the P-Cygni minima (i.e. the blueshifted absorption) of the spectral lines. In SNe, the faster material is outside (due to homologous expansion), and the measured photospheric expansion velocities decrease with time as deeper internal material is revealed (a power law evolution of $v \propto t^{-0.464}$ is typically seen, where v is the observed expansion velocity at time t from explosion[21]). For iPTF14hls, the observed slow spectral evolution indicates that the photosphere remains at higher-velocity material for longer times compared with IIP SNe (Fig. 3). A central engine like the spindown of a magnetar[5,6] or fallback accretion onto a black hole[7,8] can explain both the additional energy component and the persistence of the photosphere at high velocities. For example, a magnetar with an initial spin period of $\approx$ 5-10 ms and a magentic field of $\approx 0.5\text{-}1 \times 10^{14}$ Gauss can produce the observed average luminosity and time scale of iPTF14hls (Extended Fig. 9). However, magnetar light curves are generally expected to be smooth[5], while the light curve of iPTF14hls has at least five distinct peaks.

Some SNe have double peaked light curves[22, 23], with the first peak likely due to the cooling of the ejecta[24] and the second peak due to radioactive ^{56}Ni decay. This mechanism can thus produce at most two peaks. SN 2009ip possibly had three peaks[25, 26], likely powered by CSM interaction, which can in principle produce an arbitrary number of light curve peaks depending on the structure of the CSM. However, as mentioned above, iPTF14hls does not show any signs of CSM interaction. In addition, the spectra during the rise to the most luminous peak show an increase of flux at all wavelengths and not just in the continuum (see Methods), as expected if the peak were powered by CSM interaction. Therefore, neither of these mechanisms can explain the unprecedented multi-peak structure seen in the light curve of iPTF14hls.

Instabilities in the accretion flow onto a black hole could produce multiple light curve peaks, as seen in active galactic nuclei. In this case, the light curve is expected to eventually settle onto a $t^{-5/3}$ decline-rate[27] if a stable accretion disk forms after the last instability. Such a decline rate is indeed observed for iPTF14hls (Fig. 1), supporting this scenario.

While a central engine can reproduce the velocity evolution of the photosphere, it is not clear how an observed velocity gradient (Fig. 3) could be maintained constant as the expanding ejecta increase their size by a factor of ≈ 6 from day 100 to day 600 (see Extended Figure 6 for an explanation of why this is problematic). If the line-forming material were ejected long before our discovery of iPTF14hls, the relative increase in radius would be much smaller, and the observed velocity evolution could simply be the very late tail of a standard $t^{-0.464}$ IIP velocity law. We fit such a power law to the Fe II 5169Å velocities (Fe lines track the photosphere more accurately than the lighter elements[28, 29]) and find that it would require the material to be ejected $\gtrsim 3500$ days prior to discovery. An eruption at that time is allowed by available pre-discovery non-detection limits (Extedned Fig. 2).

The physical radius of the photosphere can be estimated at any given time t since explosion either as the radius of a blackbody sphere which fits the continuum emission spectral shape, or as $v{\cdot}t$, where v is the observed expansion velocity of the material at the position of the photosphere (as measured form the P-Cygni minima in the spectral lines) at time t (neglecting the radius of the progenitor star and assuming no acceleration after a few expansion doubling times). The equivalence of these two methods for tracing the photospheric radius is accurate up to a temperature-dependent factor known as the "blackbody dilution factor"[30] which typically has a value of order unity for the temperatures measured for iPTF14hls[31, 28]. This equivalence of the two methods for measuring the photospheric radius has been demonstrated many times and is the basis of the Expanding Photosphere Method (EPM)[30] for constraining cosmological distances to SNe IIP[32, 33, 34, 21, 29].

If the line-emitting material of iPTF14hls were indeed ejected $\gtrsim 3500$ days prior to discovery, its current radius would be $\gtrsim 10^{17}\,\mathrm{cm}$ (using the Fe II 5169Å velocity of $\approx 4000\,\mathrm{km\,s^{-1}}$), requiring a mass of $\gtrsim 200\,\mathrm{M}_{\odot}$ to remain optically thick and produce the spectral lines (see Methods). Such a large mass ejection prior to core collapse could be the result of a pulsational pair instability event[9], assuming that mechanism can account for the required $\gtrsim 10^{52}\,\mathrm{erg}$ in kinetic energy needed to eject such a shell at the velocities observed today.

The blackbody-inferred radius, on the other hand, is a few times $10^{15}\,\mathrm{cm}$ (Fig. 4), much smaller than the inferred radius at which the lines are formed. Even if the line-emitting material were ejected at discovery, the $v{\cdot}t$-inferred photospheric radius is still larger than the blackbody-inferred photospheric radius by over an order of magnitude, and growing (Fig. 4). The blackbody dilution factor is not large enough to explain the discrepancy[31, 28] or its increasing nature (the dilution factor depends on the photospheric temperature, which is roughly constant in iPTF14hls). It remains a puzzle why the two radii are so different from each other for iPTF14hls (see Methods), though similar behavior has been seen for the Type IIb SN 2011dh[35].

To our knowledge, iPTF14hls is the only SN ever discovered to show long-lived slowly-evolving IIP-like emission. The PTF and iPTF surveys alone have discovered 631 Type II SNe, indicating that iPTF14hls-like events could be 10^{-3} of the Type II SN rate. Since luminous long-lived varying events are easier to detect in transient surveys compared to normal SNe, the true volumetric rate of iPTF14hls-like events could be much lower. On the other hand, we can not rule out whether such events were discovered in the past but dismissed as normal IIP SNe after one spectrum with no subsequent followup. It is therefore not possible to calculate a precise rate for iPTF14hls-like events, but whatever the explosion channel, it must be extremely rare.

Our discovery of a new explosion channel for hydrogen-rich stars requires refinement of existing explosion scenarios, or the development of a new scenario, that can: (1) produce the same spectral signatures as common Type IIP SNe but with an evolution slowed down by a factor of $\approx 6 - 10$; (2) inject energy to prolong the light curve by a factor $\gtrsim 6$ while not introducing narrow-line spectral features or strong radio and x-ray emission indicative of CSM interaction; (3)

produce at least five peaks in the light curve; (4) decouple the deduced line-forming photosphere from the continuum photosphere; and (5) maintain a photospheric phase with a constant line-velocity gradient for over 600 days. Magnetar spindown can reproduce properties (1) and (2), and black hole accretion could in addition reproduce property (3). It is not clear if any existing SN model can reproduce properties (4) and (5). A pre-explosion high-velocity ejection of $\approx 200\,\mathrm{M}_\odot$ of hydrogen-rich material may complete the scenario, but detailed modeling is required to test this hypothesis.

iPTF14hls is an ongoing event. When it finally becomes nebular, new clues as to the nature of the progenitor star and the explosion mechanism may be revealed. Interpreting the unique observational properties of this rare SN may have implications for our understanding of the common class of SNe IIP and their use as cosmological distance indicators through the EPM method, as well as for our understanding of the late evolutionary stages of massive hydrogen-rich stars in the local Universe and the production rate of black holes.

1. Popov, D. V. An analytical model for the plateau stage of Type II supernovae. *The Astrophysical Journal* **414**, 712 (1993). URL `http://adsabs.harvard.edu/doi/10.1086/173117`.

2. Kasen, D. & Woosley, S. E. Type II Supernovae: Model Light Curves and Standard Candle Relationships. *The Astrophysical Journal* **703**, 2205–2216 (2010). URL `http://arxiv.org/abs/0910.1590http://dx.doi.org/10.1088/0004-637X/703/2/2205`. `0910.1590`.

3. Nakar, E., Poznanski, D. & Katz, B. The importance of 56Ni in shaping the light curves of type II supernovae. *The Astrophysical Journal* **823** (2016). URL http://arxiv.org/abs/1506.07185http://dx.doi.org/10.3847/0004-637X/823/2/127. 1506.07185.

4. Ostriker, J. P. & Gunn, J. E. On the Nature of Pulsars. I. Theory. *The Astrophysical Journal* **157**, 1395 (1969). URL http://adsabs.harvard.edu/doi/10.1086/150160.

5. Kasen, D. & Bildsten, L. SUPERNOVA LIGHT CURVES POWERED BY YOUNG MAGNETARS. *The Astrophysical Journal* **717**, 245–249 (2010). URL http://adsabs.harvard.edu/abs/2010ApJ...717..245K.

6. Woosley, S. E. BRIGHT SUPERNOVAE FROM MAGNETAR BIRTH. *The Astrophysical Journal* **719**, L204–L207 (2010). URL http://adsabs.harvard.edu/abs/2010ApJ...719L.204W.

7. Colgate, S. A. Neutron-Star Formation, Thermonuclear Supernovae, and Heavy-Element Reimplosion. *The Astrophysical Journal* **163**, 221 (1971). URL http://adsabs.harvard.edu/doi/10.1086/150760.

8. Dexter, J. & Kasen, D. SUPERNOVA LIGHT CURVES POWERED BY FALLBACK ACCRETION. *The Astrophysical Journal* **772**, 30 (2013). URL http://stacks.iop.org/0004-637X/772/i=1/a=30?key=crossref.6ebc8a4f6831234f803ea155f05e61e2.

9. Woosley, S. E., Blinnikov, S. & Heger, A. Pulsational pair instability as an explanation for the most luminous supernovae. *Nature, Volume 450, Issue 7168, pp. 390-392 (2007).* **450**, 390–392 (2007). URL `http://arxiv.org/abs/0710.3314http://dx.doi.org/10.1038/nature06333`. `0710.3314`.

10. Rau, A. *et al.* Exploring the Optical Transient Sky with the Palomar Transient Factory. *Publications of the Astronomical Society of the Pacific* **121**, 1334–1351 (2009). URL `http://arxiv.org/abs/0906.5355http://dx.doi.org/10.1086/605911`. `0906.5355`.

11. Law, N. M. *et al.* The Palomar Transient Factory: System Overview, Performance and First Results. *Publications of the Astronomical Society of the Pacific* **121**, 1395–1408 (2009). URL `http://arxiv.org/abs/0906.5350http://dx.doi.org/10.1086/648598`. `0906.5350`.

12. Drake, A. J. *et al.* First Results from the Catalina Real-time Transient Survey. *The Astrophysical Journal* **696**, 870–884 (2009). URL `http://arxiv.org/abs/0809.1394http://dx.doi.org/10.1088/0004-637X/696/1/870`. `0809.1394`.

13. Li, W., Wang, X. & Zhang, T. Spectroscopic Classification of CSS141118:092034+504148 as a Type II-P Supernova. *The Astronomer's Telegram* **6898** (2015).

14. Planck Collaboration *et al.* Planck 2015 results. XIII. Cosmological parameters (2015). `1502.01589`.

15. Tremonti, C. A. *et al.* The Origin of the MassMetallicity Relation: Insights from 53,000 Starforming Galaxies in the Sloan Digital Sky Survey. *The Astrophysical Journal* **613**, 898–913 (2004). URL http://adsabs.harvard.edu/abs/2004ApJ...613..898T.

16. Bersten, M. C. & Hamuy, M. BOLOMETRIC LIGHT CURVES FOR 33 TYPE II PLATEAU SUPERNOVAE. *The Astrophysical Journal* **701**, 200–208 (2009). URL http://adsabs.harvard.edu/abs/2009ApJ...701..200B.

17. Rest, A. *et al.* Pushing the Boundaries of Conventional Core-Collapse Supernovae: The Extremely Energetic Supernova SN 2003ma. *The Astrophysical Journal, Volume 729, Issue 2, article id. 88, 18 pp. (2011).* **729** (2011). URL http://arxiv.org/abs/0911.2002http://dx.doi.org/10.1088/0004-637X/729/2/88. 0911.2002.

18. Schlegel, . A new subclass of Type II supernovae? *Monthly Notices of the Royal Astronomical Society (ISSN 0035-8711)* **244**, 269–271 (1990). URL http://adsabs.harvard.edu/abs/1990MNRAS.244..269S.

19. Chugai, N. N. Evidence for energizing of H emission in type II supernovae by ejecta-wind interaction. *Monthly Notices of the Royal Astronomical Society* **250**, 513–518 (1991). URL http://adsabs.harvard.edu/abs/1991MNRAS.250..513C.

20. Kiewe, M. *et al.* CALTECH CORE-COLLAPSE PROJECT (CCCP) OBSERVATIONS OF TYPE IIn SUPERNOVAE: TYPICAL PROPERTIES AND IMPLICATIONS FOR THEIR PROGENITOR STARS. *The Astrophysical Journal* **744**, 10 (2012). URL http://adsabs.harvard.edu/abs/2012ApJ...744...10K.

21. Nugent, P. *et al.* Toward a Cosmological Hubble Diagram for Type IIP Supernovae. *The Astrophysical Journal* **645**, 841–850 (2006). URL `http://adsabs.harvard.edu/abs/2006ApJ...645..841N`.

22. Richmond, M. W. *et al.* UBVRI photometry of SN 1993J in M81: The first 120 days. *The Astronomical Journal* **107**, 1022 (1994). URL `http://adsabs.harvard.edu/abs/1994AJ....107.1022R`.

23. Arcavi, I. *et al.* SN 2011dh: DISCOVERY OF A TYPE IIb SUPERNOVA FROM A COMPACT PROGENITOR IN THE NEARBY GALAXY M51. *The Astrophysical Journal* **742**, L18 (2011). URL `http://adsabs.harvard.edu/abs/2011ApJ...742L..18A`.

24. Nakar, E. & Piro, A. L. SUPERNOVAE WITH TWO PEAKS IN THE OPTICAL LIGHT CURVE AND THE SIGNATURE OF PROGENITORS WITH LOW-MASS EXTENDED ENVELOPES. *The Astrophysical Journal* **788**, 193 (2014). URL `http://adsabs.harvard.edu/abs/2014ApJ...788..193N`.

25. Smith, N., Mauerhan, J. & Prieto, J. SN 2009ip and SN 2010mc: Core-collapse Type IIn supernovae arising from blue supergiants. *Monthly Notices of the Royal Astronomical Society, Volume 438, Issue 2, p.1191-1207* **438**, 1191–1207 (2013). URL `http://arxiv.org/abs/1308.0112http://dx.doi.org/10.1093/mnras/stt2269`. `1308.0112`.

26. Graham, M. L. *et al.* Clues To The Nature of SN 2009ip from Photometric and Spectroscopic Evolution to Late Times. *The Astrophysical Journal, Volume 787, Issue 2, article id. 163,*

16 pp. (2014). **787** (2014). URL http://arxiv.org/abs/1402.1765http://dx.doi.org/10.1088/0004-637X/787/2/163. 1402.1765.

27. Phinney, . Manifestations of a Massive Black Hole in the Galactic Center. *The Center of the Galaxy: Proceedings of the 136th Symposium of the International Astronomical Union* (1989). URL http://adsabs.harvard.edu/abs/1989IAUS..136..543P.

28. Dessart, L. & Hillier, D. J. Distance determinations using type II supernovae and the expanding photosphere method. *Astronomy and Astrophysics* **439**, 671–685 (2005). URL http://www.edpsciences.org/10.1051/0004-6361:20053217.

29. Poznanski, D. *et al.* IMPROVED STANDARDIZATION OF TYPE II-P SUPERNOVAE: APPLICATION TO AN EXPANDED SAMPLE. *The Astrophysical Journal* **694**, 1067–1079 (2009). URL http://adsabs.harvard.edu/abs/2009ApJ...694.1067P.

30. Kirshner, R. P. & Kwan, J. The envelopes of type II supernovae. *The Astrophysical Journal* **197**, 415 (1975). URL http://adsabs.harvard.edu/abs/1975ApJ...197..415K.

31. Eastman, R. G., Schmidt, B. P. & Kirshner, R. The Atmospheres of Type II Supernovae and the Expanding Photosphere Method. *The Astrophysical Journal* **466**, 911 (1996). URL http://adsabs.harvard.edu/doi/10.1086/177563.

32. Schmidt, B. P. *et al.* The distances to five Type II supernovae using the expanding photosphere method, and the value of H[SUB]0[/SUB]. *The Astrophysical Journal* **432**, 42 (1994). URL http://adsabs.harvard.edu/doi/10.1086/174546.

33. Hamuy, M. *et al.* The Distance to SN 1999em from the Expanding Photosphere Method. *The Astrophysical Journal* **558**, 615–642 (2001). URL http://stacks.iop.org/0004-637X/558/i=2/a=615.

34. Leonard, D. *et al.* The Distance to SN 1999em in NGC 1637 from the Expanding Photosphere Method. *Publications of the Astronomical Society of the Pacific* **114**, 35–64 (2002). URL http://adsabs.harvard.edu/abs/2002PASP..114...35L.

35. Ergon, M. *et al.* Optical and near-infrared observations of SN 2011dh The first 100 days. *Astronomy & Astrophysics* **562**, A17 (2014). URL http://www.aanda.org/10.1051/0004-6361/201321850.

36. Cenko, S. B. *et al.* The Automated Palomar 60 Inch Telescope. *Publications of the Astronomical Society of the Pacific* **118**, 1396–1406 (2006). 0608323.

37. Brown, T. M. *et al.* Las Cumbres Observatory Global Telescope Network. *Publications of the Astronomical Society of Pacific, Volume 125, Issue 931, pp. 1031-1055 (2013).* **125**, 1031–1055 (2013). URL http://arxiv.org/abs/1305.2437http://dx.doi.org/10.1086/673168. 1305.2437.

38. Laher, R. R. *et al.* IPAC Image Processing and Data Archiving for the Palomar Transient Factory. *Publications of the Astronomical Society of the Pacific* **126**, 674–710 (2014). 1404.1953.

39. Sullivan, M. *et al.* Photometric Selection of High-Redshift Type Ia Supernova Candidates. *The Astronomical Journal* **131**, 960–972 (2006). 0510857.

40. Ahn, C. P. *et al.* The Tenth Data Release of the Sloan Digital Sky Survey: First Spectroscopic Data from the SDSS-III Apache Point Observatory Galactic Evolution Experiment. *The Astrophysical Journal Supplement Series* **211** (2014). 1307.7735.

41. Fremling, C. *et al.* PTF12os and iPTF13bvn. Two stripped-envelope supernovae from low-mass progenitors in NGC 5806. *eprint arXiv:1606.03074* (2016). URL http://arxiv.org/abs/1606.03074. 1606.03074.

42. Jenness, T. & Economou, F. ORAC-DR: A generic data reduction pipeline infrastructure. *Astronomy and Computing* **9**, 40–48 (2015). 1410.7509.

43. Valenti, S. *et al.* The diversity of Type II supernova versus the similarity in their progenitors. *Monthly Notices of the Royal Astronomical Society, Volume 459, Issue 4, p.3939-3962* **459**, 3939–3962 (2016). URL http://arxiv.org/abs/1603.08953http://dx.doi.org/10.1093/mnras/stw870. 1603.08953.

44. Henden, A. A., Welch, D. L., Terrell, D. & Levine, S. E. The AAVSO Photometric All-Sky Survey (APASS) (2009).

45. Aihara, H. *et al.* The Eighth Data Release of the Sloan Digital Sky Survey: First Data from SDSS-III. *The Astrophysical Journal Supplement Series* **193** (2011). 1101.1559.

46. Schlafly, E. F. & Finkbeiner, D. P. Measuring Reddening with SDSS Stellar Spectra and Recalibrating SFD. *The Astrophysical Journal, Volume 737, Issue 2, article id. 103, 13 pp. (2011).* **737** (2011). URL http://arxiv.org/abs/1012.4804http://dx.doi.org/10.1088/0004-637X/737/2/103. 1012.4804.

47. Foreman-Mackey, D., Hogg, D. W., Lang, D. & Goodman, J. emcee: The MCMC Hammer. *Publications of the Astronomical Society of Pacific, Volume 125, Issue 925, pp. 306-312 (2013).* **125**, 306–312 (2012). URL `http://arxiv.org/abs/1202.3665http://dx.doi.org/10.1086/670067`. `1202.3665`.

48. Oke, J. B. *et al.* The Keck Low-Resolution Imaging Spectrometer. *Publications of the Astronomical Society of the Pacific* **107**, 375 (1995). URL `http://www.jstor.org/stable/10.2307/40680546`.

49. Faber, S. M. *et al.* The DEIMOS spectrograph for the Keck II Telescope: integration and testing. In Iye, M. & Moorwood, A. F. M. (eds.) *Instrument Design and Performance for Optical/Infrared Ground-based Telescopes. Edited by Iye, Masanori; Moorwood, Alan F. M. Proceedings of the SPIE, Volume 4841, pp. 1657-1669 (2003).*, vol. 4841, 1657–1669 (2003). URL `http://proceedings.spiedigitallibrary.org/proceeding.aspx?articleid=874397`.

50. Oke, J. B. & Gunn, J. E. An Efficient Low Resolution and Moderate Resolution Spectrograph for the Hale Telescope. *Publications of the Astronomical Society of the Pacific* **94**, 586 (1982). URL `http://www.jstor.org/stable/10.2307/40677999`.

51. Cooper, M. C., Newman, J. A., Davis, M., Finkbeiner, D. P. & Gerke, B. F. spec2d: DEEP2 DEIMOS Spectral Pipeline. *Astrophysics Source Code Library, record ascl:1203.003* (2012).

52. Newman, J. A. *et al.* The DEEP2 Galaxy Redshift Survey: Design, Observations, Data Reduction, and Redshifts. *The Astrophysical Journal Supplement, Volume 208, Issue 1, article*

id. 5, 57 pp. (2013). **208** (2012). URL http://arxiv.org/abs/1203.3192http://dx.doi.org/10.1088/0067-0049/208/1/5. 1203.3192.

53. Howell, D. A. *et al.* Gemini Spectroscopy of Supernovae from SNLS: Improving High Redshift SN Selection and Classification. *The Astrophysical Journal, Volume 634, Issue 2, pp. 1190-1201.* **634**, 1190–1201 (2005). URL http://arxiv.org/abs/astro-ph/0509195http://dx.doi.org/10.1086/497119. 0509195.

54. Dessart, L. *et al.* Type II-Plateau supernovae as metallicity probes of the Universe. *Monthly Notices of the Royal Astronomical Society, Volume 440, Issue 2, p.1856-1864* **440**, 1856–1864 (2014). URL http://arxiv.org/abs/1403.1167http://dx.doi.org/10.1093/mnras/stu417. 1403.1167.

55. Taddia, F. *et al.* Metallicity from Type II Supernovae from the (i)PTF. *Astronomy & Astrophysics, Volume 587, id.L7, 6 pp.* **587** (2016). URL http://arxiv.org/abs/1602.01433http://dx.doi.org/10.1051/0004-6361/201527983. 1602.01433.

56. Nordin, J. *et al.* Spectral properties of Type Ia supernovae up to z˜0.3. *Astronomy and Astrophysics, Volume 526, id.A119, 31 pp.* **526** (2011). URL http://arxiv.org/abs/1011.6227http://dx.doi.org/10.1051/0004-6361/201015705. 1011.6227.

57. Burrows, D. N. *et al.* The Swift X-ray Telescope. *Space Science Reviews* **120**, 165–195 (2005). URL http://arxiv.org/abs/astro-ph/0508071http://dx.doi.org/10.1007/s11214-005-5097-2. 0508071.

58. Gehrels, N. *et al.* The <i>Swift</i> GammaRay Burst Mission. *The Astrophysical Journal* **611**, 1005–1020 (2004). URL http://stacks.iop.org/0004-637X/611/i=2/a=1005.

59. Evans, P. A. *et al.* An online repository of Swift/XRT light curves of GRBs. *Astronomy and Astrophysics* **469**, 379–385 (2007). URL http://arxiv.org/abs/0704.0128http://dx.doi.org/10.1051/0004-6361:20077530. 0704.0128.

60. Evans, P. A. *et al.* Methods and results of an automatic analysis of a complete sample of Swift-XRT observations of GRBs. *Monthly Notices of the Royal Astronomical Society* **397**, 1177–1201 (2009). URL http://arxiv.org/abs/0812.3662http://dx.doi.org/10.1111/j.1365-2966.2009.14913.x. 0812.3662.

61. Willingale, R., Starling, R. L. C., Beardmore, A. P., Tanvir, N. R. & O'Brien, P. T. Calibration of X-ray absorption in our Galaxy. *Monthly Notices of the Royal Astronomical Society* **431**, 394–404 (2013). URL http://arxiv.org/abs/1303.0843http://dx.doi.org/10.1093/mnras/stt175. 1303.0843.

62. Alam, S. *et al.* The Eleventh and Twelfth Data Releases of the Sloan Digital Sky Survey: Final Data from SDSS-III. *The Astrophysical Journal Supplement Series, Volume 219, Issue 1, article id. 12, 27 pp. (2015).* **219** (2015). URL http://arxiv.org/abs/1501.00963http://dx.doi.org/10.1088/0067-0049/219/1/12. 1501.00963.

63. Cutri, R. M. & et Al. VizieR Online Data Catalog: AllWISE Data Release (Cutri+ 2013). *VizieR On-line Data Catalog: II/328. Originally published in: 2013yCat.2328....0C* **2328**

(2013).

64. Perley, D. A. *et al.* A Population of Massive, Luminous Galaxies Hosting Heavily Dust-Obscured Gamma-Ray Bursts: Implications for the Use of GRBs as Tracers of Cosmic Star Formation. *The Astrophysical Journal, Volume 778, Issue 2, article id. 128, 35 pp. (2013).* **778** (2013). URL http://arxiv.org/abs/1301.5903http://dx.doi.org/10.1088/0004-637X/778/2/128. 1301.5903.

65. Bruzual, G. & Charlot, S. Stellar population synthesis at the resolution of 2003. *Monthly Notices of the Royal Astronomical Society, Volume 344, Issue 4, pp. 1000-1028.* **344**, 1000–1028 (2003). URL http://arxiv.org/abs/astro-ph/0309134http://dx.doi.org/10.1046/j.1365-8711.2003.06897.x. 0309134.

66. Filippenko, A. V. The importance of atmospheric differential refraction in spectrophotometry. *Publications of the Astronomical Society of the Pacific* **94**, 715 (1982). URL http://www.jstor.org/stable/10.2307/40678026.

Acknowledgements We are grateful to D. Leonard and D. Poznanski for discussions. This research is funded in part by the Gordon and Betty Moore Foundation through Grant GBMF5076 to LB and DK and by the National Science Foundation under grant PHY 11-25915. DAH, CM, and GH are supported by NSF grant 1313484. JS gratefully acknowledges support from the Knut and Alice Wallenberg Foundation. This paper made use of data from Las Cumbres Observatory Global Telescope Network. This work is partly based on observations made with the Nordic Optical Telescope, operated by the Nordic Optical Telescope Scientific Association at the Observatorio del Roque de los Muchachos, La Palma, Spain, of the Instituto de Astrofisica de Canarias. Some data presented here were obtained with ALFOSC, which is provided by the Instituto de Astrofisica de Andalucia (IAA) under a joint agreement with the University of Copenhagen and NOTSA. This work is partly based on observations made with DOLoRes on TNG. These results made use of the Discovery Channel Telescope (DCT) at Lowell Observatory. Lowell is a private, non-profit institution dedicated to astrophysical research and public appreciation of astronomy and operates the DCT in partnership with Boston University, the University of Maryland, the University of Toledo, Northern Arizona University and Yale University. The upgrade of the DeVeny optical spectrograph has been funded by a generous grant from John and Ginger Giovale.

Competing Interests The authors declare that they have no competing financial interests.

Author Contributions TBD

Correspondence Correspondence and requests for materials should be addressed to Iair Arcavi (email: arcavi@gmail.com).

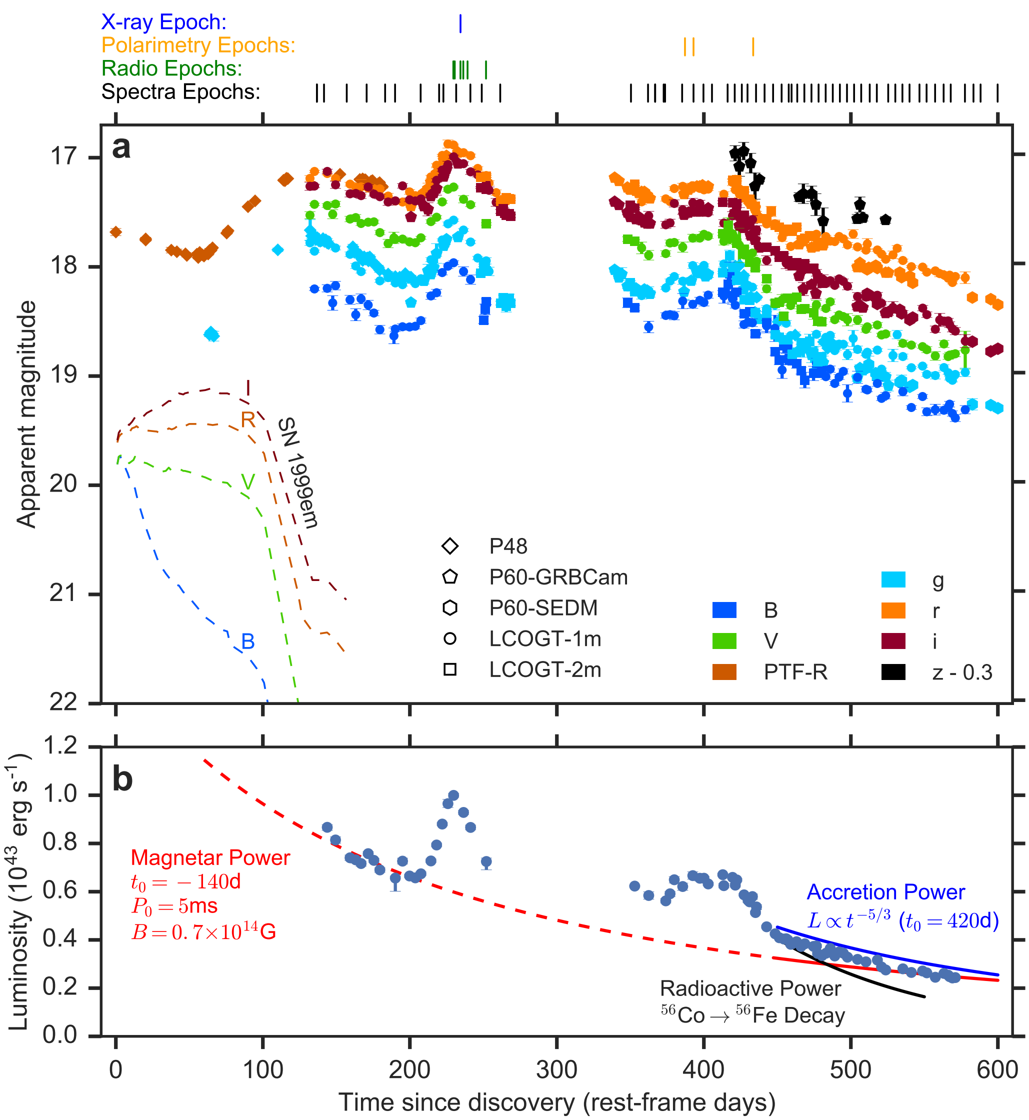

Figure 1 **Christofer working on final P60 photometry** Multi-band optical light curves of iPTF14hls (**a**; see Methods for telescope names). The prototypical Type IIP SN 1999em is shown for comparison (dashed lines)[34], matched to the absolute magnitude displayed on the right axis. Photometric points from the same day, instrument and filter are averaged for clarity. The SEDM i-band data is shifted by $+0.3$ magnitudes to compensate for filter differences with the other instruments. The upper tick marks denote epochs of optical

spectroscopic (black), radio (green), polarimetry (orange) and X-ray (blue) observations. The last pre-discovery non-detection of iPTF14hls was obtained by iPTF approximately 139 days before discovery (not shown), leaving the explosion time of iPTF14hls not well constrained. Even so, iPTF14hls remains luminous substantially longer than a normal IIP and displays evidence for at least five distinct light-curve peaks (at approximately 140, 220 and 410 days after discovery, as well as at least one peak before discovery, as indicated by the R-band light curve, and one while the SN was behind the sun between days 260 and 340 after discovery). iPTF14hls remains roughly constant in color, whereas normal IIP SNe decline faster in the bluer bands due to increasing iron-line opacity. The bolometric light curve of iPTF14hls (**b**) is deduced from blackbody fits to the broad-band $BVgi$ photometry. The late-time decline is slower than the radioactive decay of ^{56}Co (which usually dominates SN light curves at these phases; black), but is consistent with both accretion power (blue; t_0 is the onset of accretion at the last peak) and magnetar spindown power (red; t_0 is the formation time of the magentar, P_0 the initial spin period and B the magnetic field of the magnetar). The magnetar model, however, is not consistent with the luminosity during the first 100 days, as implied by the R-band observations at that epoch (**a**).

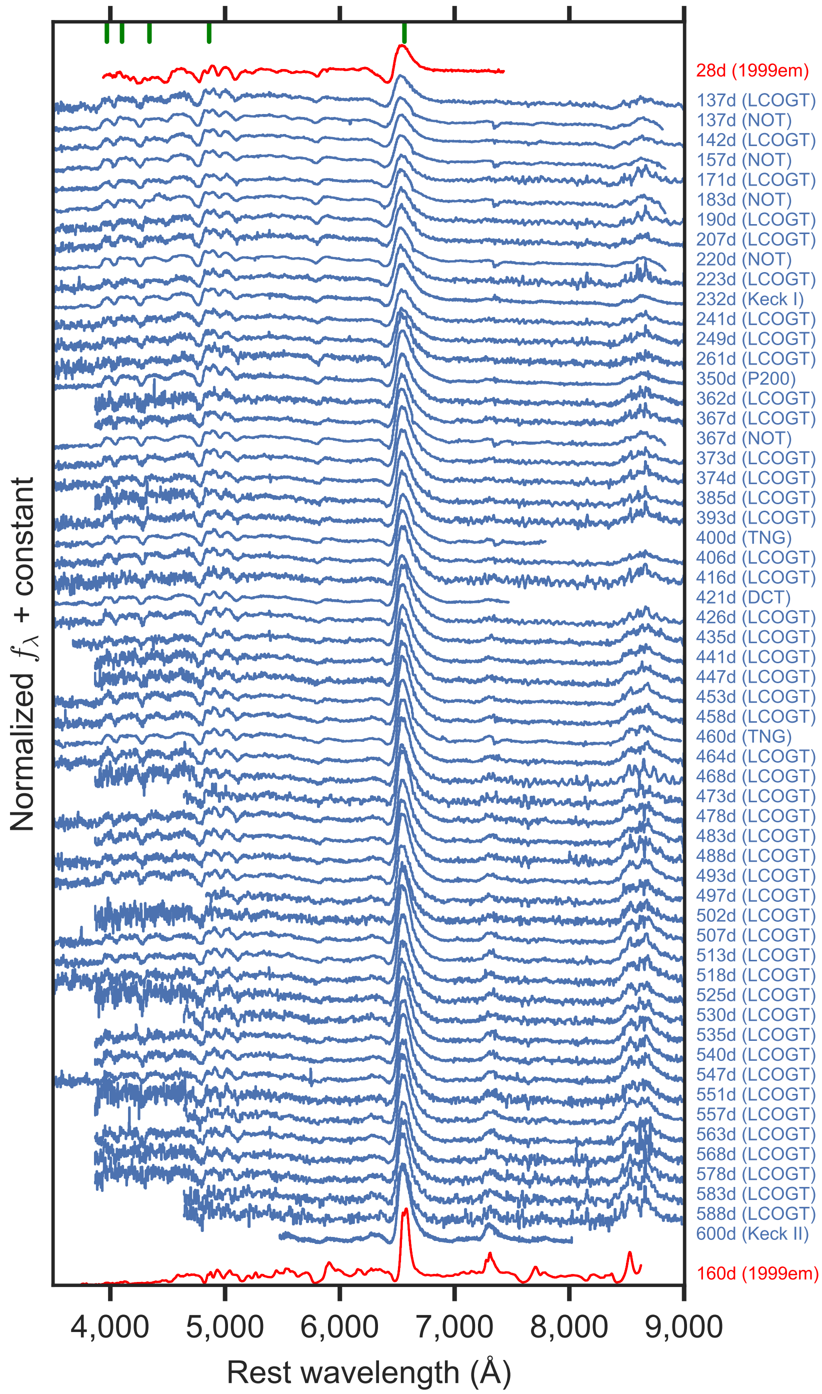

Figure 2 Optical spectra of iPTF14hls (blue) expressed in terms of normalized flux density as a function of rest-frame wavelength. The spectra are binned in wavelength and

shifted in flux for clarity. Phases are noted in rest-frame days since discovery on the right axis, with the telescope used to obtain the spectrum in parentheses (see Methods for details). Spectra of the prototypical Type IIP SN 1999em[34] (red) are shown for comparison with phases noted in rest-frame days since explosion. Balmer series hydrogen line wavelengths are denoted in green tick marks at the top. iPTF14hls is similar spectroscopically to a normal Type IIP SN but evolves much slower. The spectral evolution is very smooth, in contrast to the multi-peaked light curve. No narrow emission lines, as signs of interaction with circumstellar material, are seen (see also Extended Figure 8).

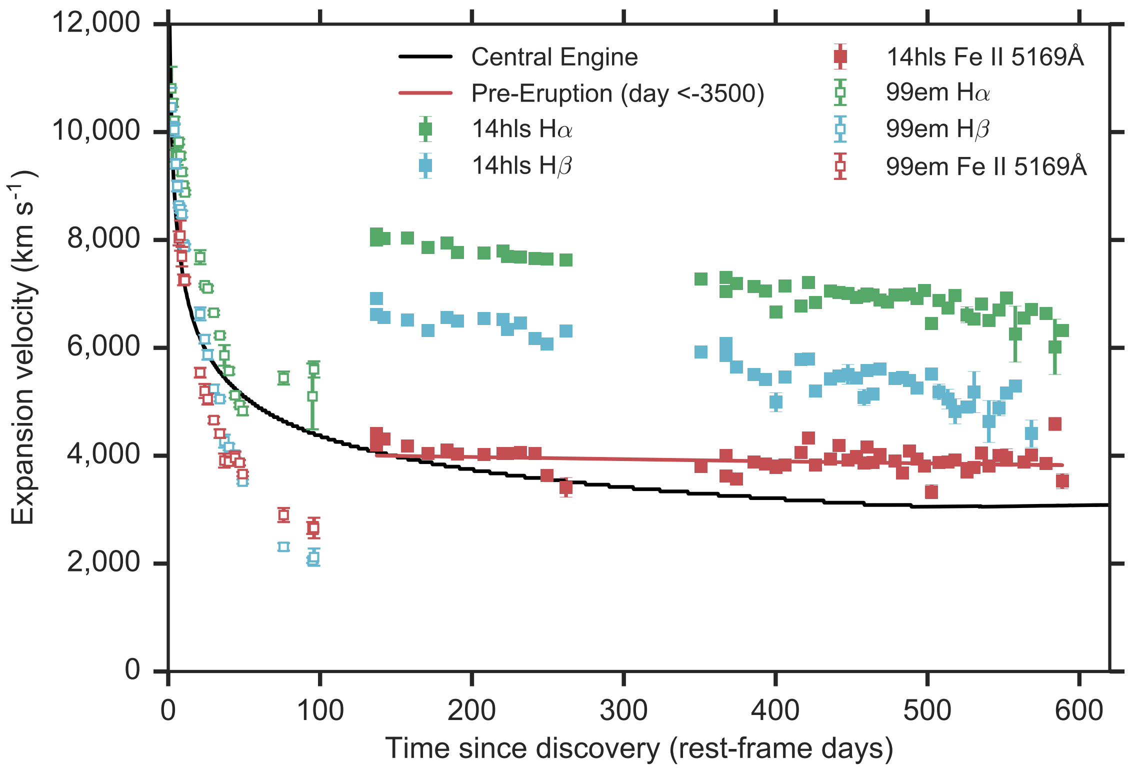

Figure 3 Expansion velocities as a function of time, measured from the P-Cygni absorption features (see Methods for details), of three different spectral lines, for iPTF14hls (filled symbols) and the prototypical Type IIP SN 1999em[34] (empty symbols). A magnetar-powered velocity evolution is shown (black) for an ejecta mass of $15\,\mathrm{M}_{\odot}$, an explosion energy of 10^{51} erg and a spindownd period of 100 days, assuming the magnetar formed at discovery. The red line is the best-fit $t^{-0.464}$ velocity decline rate observed in normal IIP SNe, without magnetar formation but requiring an envelope ejection date at least ≈ 3500 days before discovery.

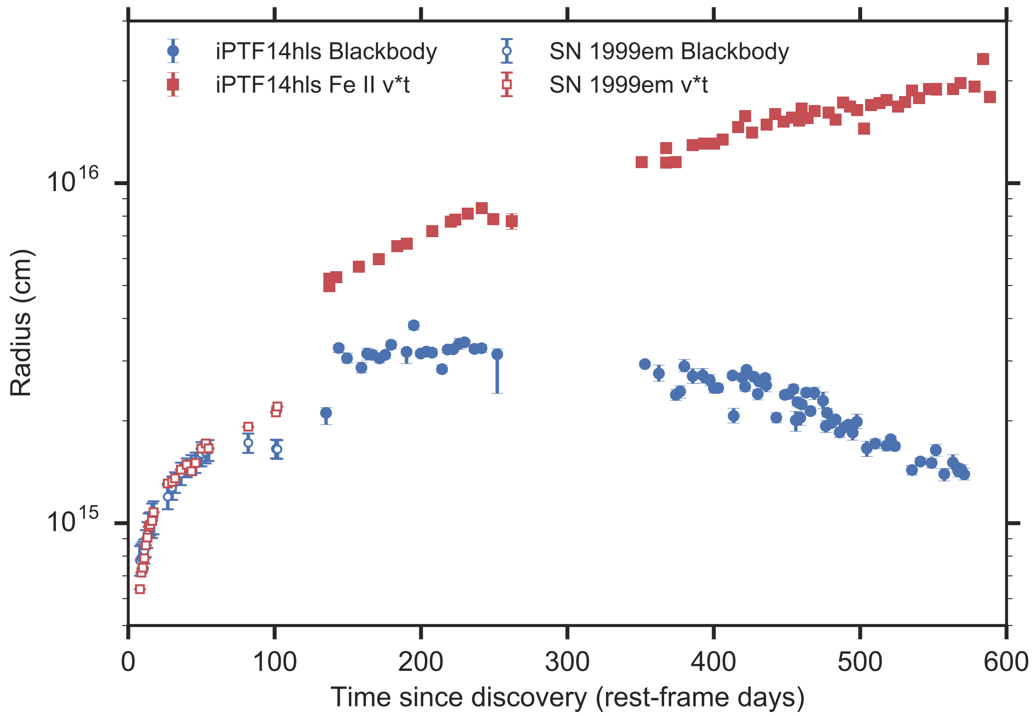

Figure 4 The photospheric radius of iPTF14hls (filled symbols) estimated in two different ways: (1) Using blackbody fits to the broad-band $BVgi$ photometry (blue) and (2) using the derived expansion velocities of Fe II 5169Å (Fig. 3) times the elapsed rest-frame time since discovery (red). The same quantities are shown for the prototypical Type IIP SN 1999em (empty symbols; after correcting for the blackbody dilution factor)[34]. For SN 1999em the radii overlap as expected, but for iPTF14hls they diverge.

Methods

Discovery The intermediate Palomar Transient Factory first detected iPTF14hls on 2014 Sep 22.53 (Extended Fig. 1). Prior to then, the field was last visited by iPTF 139 days earlier. The source was observed by iPTF again on 2014 Oct 13, Oct 31, Nov 4 and Nov 10 before being saved and given a name as part of routine iPTF transient scanning. On 2015 Feb 3, upon routine LCOGT re-scanning of previously saved iPTF candidates, we noticed the peculiar decline then rise of the light curve (but were unaware of the public classification of this target as a Type IIP SN)[13], and began an extensive campaign of spectroscopic and multi-band photometric followup.

Optical Photometry Images were obtained with the Palomar 48-inch Oschin Schmidt telescope (P48), the Palomar 60-inch telescope (P60)[36] using both the GRBCam and SED Machine (SEDM) instruments, and the Las Cumbres Observatory Global Telescope (LCOGT)[37] network 1-meter and 2-meter telescopes. P48 images were first pre-processed by the Infrared Processing and Analysis Center (IPAC)[38]. Image subtraction and PSF fitting was then performed[39] using pre-explosion images as templates. Magnitudes were calibrated to observations of the same field by the Sloan Digital Sky Survey (SDSS) DR10[40]. P60 images were pre-processed using a PyRAF-based pipeline[36]. Image subtraction, photometry extraction and calibration were performed with the `FPipe` pipeline[41] using SDSS images as references. LCOGT images were pre-processed using the Observatory Reduction and Acquisition Control Data Reduction pipeline (ORAC-DR)[42] up to 2016 May 4, and using the custom Python-based `BANZAI` pipeline afterwards. Photometry was then extracted using the PyRAF-based `lcogtsnpipe` pipeline[43] to perform PSF fitting and calibration to the AAVSO Photometric All-Sky Survey[44] for BV-band data and SDSS DR8[45] for gri-band data. We correct all photometry for Milky Way extinction[46] extracted via the NASA Extragalactic Database (NED).

Blackbody Fitting We fit a blackbody SED to every epoch of LCOGT photometry containing at least three of the $BVgi$ filters obtained within 0.4 days of each other (we exclude r-band data from the fits due to contamination from the Hα line). For each epoch we perform a blackbody fit using Markov Chain Monte Carlo simulations, through the Python `emcee` package[47], to estimate the blackbody temperature and radius at the measured distance to iPTF14hls of 156.2 Mpc.

Polarimetry **Final version of this text TDB Jesper / Giorgos.** We observed iPTF14hls with the the Andalucia Faint Object Spectrograph and Camera (ALFOSC) mounted on the 2.5-meter Nordic Optical Telescope (NOT) in polarimetric mode on 2015 Oct 28, Nov 03 and Dec 15. We use a 1/2 wave plate in the FAPOL unit and a calcite plate mounted in the aperture wheel. The calcite plate provides the simultaneous measurement of the ordinary and the extraordinary components of two orthogonally polarized beams **[to be confirmed by Giorgos]**. We observed in 4 different retarder angles (0, 22.5, 45, 67.5 deg) at each epoch, using the V- and R-band filters. The data were reduced in a standard manner, using bias frames and flat-fields without the polarisation units in the light path. **The conditions were varying. Do we want to say anything about that?** We then performed aperture photometry on each frame on both the ordinary and extraordinary beam, on both the SN and **X** comparison stars. By taking the ratio of fluxes and following standard procedures[?], we are able to measure the Stokes parameters (for both the SN and the comparison stars) **The difficult part is the determination of the ISP**. The main limitation of the instrument is the small field of view that only included 2 **1-4?** suitable objects, which does not allow for an accurate determination of the ISP. **We estimate the ISP to be ... We do not detect any significant polarisation for iPTF14hls. The measured polarisation is X%, implying ... within the accuracy that we can obtain we cannot detect any measurable evolution...**

Optical Spectroscopy Spectra of iPTF14hls were obtained with the Floyds instrument mounted on the northern LCOGT 2-meter telescope[37], the Andalucia Faint Object Spectrograph and Camera (ALFOSC) mounted on the 2.5-meter Nordic Optical Telescope (NOT), the Device Optimized for the LOw RESolution (DOLoRes) mounted on the 3.6-meter Telescopio Nazionale Galileo (TNG), the Low Resolution Imaging Spectrometer (LRIS)[48] mounted on the Keck I 10-meter telescope, the DEep Imaging Multi-Object Spectrograph (DEIMOS)[49] mounted on the Keck II 10-meter telescope, the Double Beam Spectropgraph (DBSP)[50] mounted on the Palomar 200-inch telescope (P200) and the DeVeny spectrograph mounted on the 4.3-meter Discovery Channel Telescope (DCT). The Floyds spectra were reduced using the PyRAF-based `floydsspec` pipeline. The ALFOSC and DOLORES spectra were reduced using custom MATLAB pipelines. The LRIS spectra were reduced using the IDL `LPipe` pipeline. The DEIMOS spectrum was reduced using a modified version of the `DEEP2` pipeline[51, 52] combined with standard PyRAF and IDL routines for trace extraction, flux calibration and telluric correction. The DBSP spectrum was reduced using custom IRAF and IDL routines. The DeVeny spectrum was reduced using standard IRAF procedures.

Spectral Fitting We fit each iPTF14hls spectrum to a library of Type II SNe (which includes a full set of SN 1999em spectra[34]) using Superfit[53]. We then calculate the average best-fit SN phase, weighing all the possible fits by their corresponding fit scores. We repeat this process for cutouts of the iPTF14hls spectra centered around the Hα, Hβ and Fe II 5169Å features (separately). The weighted-average best-fit phases for each cutout are presented in Extended Figure 3. iPTF14hls can be seen to evolve slower than other Type II SNe by approximately a factor of 10 when considering the entire spectrum, as well as when considering the Hβ and the Fe II 5169Å features separately, and by a factor of $6-7$ when considering the Hα emission feature separately.

Expansion Velocity Measurements Expansion velocities for different elements were measured by fitting a parabola around the minimum of the absorption feature of their respective P-Cygni profiles. The difference between the minimum of the best-fit parabola and the rest-wavelength of the line was translated to an expansion velocity. The end points of each parabola fit were chosen manually per line, so that they would remain the same for all spectra. Errors on the velocities were estimated by randomly varying these endpoints by ± 5Å around their original values. The Fe II 5169Å velocities were then fit to a $t^{-0.464}$ power law using Markov Chain Monte Carlo simulations, through the Python `emcee` package[47], with the ejection time and velocity normalization as free parameters.

Expansion Velocity Interpretations In a SN, the ejecta are in homologous expansion, that is, the radius of the ejecta at time t evolves as $r = v{\cdot}t$ with faster material at larger radii. Even for perfectly mixed ejecta, at any given time spectral lines of different elements form in different regions. Specifically, the Fe lines are formed at smaller radii than the H lines and therefore display a lower velocity. This is also the case in iPTF14hls. As time passes and the ejecta expand and recombine, the line-forming region of each element moves inward in mass to a region where the outflow is slower. This is why the velocity of all lines is observed to decrease with time. Thus, following the line velocity over a large range of time (and hence mass coordinates) provides a "scan" of the velocity profile over a large range of the ejecta. Although different lines are formed at different regions, all line-forming regions scan the velocity of the same ejecta. Therefore if there is a significant velocity gradient in the ejecta, we expect to see both a significant difference between the velocity of Fe lines vs. H lines and significant evolution in the velocity of each line when the outflow radius changes significantly. There two features are seen clearly in the typical case of SN 1999em (Extended Data Fig. 6). However, this doesnt seems to be the case in iPTF14hls. On one hand there is a significant difference between the H and Fe line velocities, indicating a large velocity gradient in the ejecta. However, on the other hand, the velocity of each line shows almost no evolution in time between days 100 and 600 after discovery. If the line-forming material were ejected just before discovery then this time span corresponds to a change by a factor of ≈ 6 in radius. In this case, the lack of observed velocity evolution indicates a very shallow velocity gradient in the ejecta, which is inconsistent with the large velocity difference between the lines. However, if the ejection of the line-forming material took place long before discovery, then the relative change in radius during the observations is small, indicating that the position of the line-forming region does not change much, thus solving the apparent contradiction. Hence, we may be observing the late tail of the standard $v \propto t^{-0.464}$ evolution, which is what we fit the Fe-line velocities with.

Metallicity Measurements The Fe II 5018Å absorption pseudo equivalent width (pEW) in Type IIP SN spectra has recently been shown to be a good proxy for the metallicity of the progenitor star[54, 55]. We measure the pEW for this line in our spectra following a standard prescription[56]. The wavelength regions we use to define the pseudo continuum are $4896 - 4916$Å on one side and $5008 - 5028$Å on the other (rest wavelength). The minimum of the Fe II 5018Å P-Cygni absorption feature lies in the range $4950 - 4970$Å. We estimate the error on the pEW measurement by randomly varying the pseudo continuum regions from a Gaussian distribution with a conservative 10Å standard deviation. The results indicate a low ($Z < 0.1\,\mathrm{Z}_{\odot}$, where $\mathrm{Z}_{\odot}$ is the solar metallicity) metallicity progenitor when compared to models[54], though no models have been made for the late epochs at which iPTF14hls was observed (Extended Figure 4).

The Added Luminosity in the Main Peak The luminosity of iPTF14hls increases by approximately 50% between rest-frame day 207 and 232 after peak (Fig. 1). Generally, CSM interaction luminosity contributes to the continuum level, while central-engine luminosity being reprocessed by the outer layers would increase both the continuum and the line luminosity equally. We find that the spectra taken on day 207 and day 232 are identical up to a global normalization factor, indicating that the increase in luminosity is equal at all wavelengths. If the increase were only to the continuum flux, then the lines would appear diluted (i.e. weaker) in the normalized flux comparison. To demonstrate this, we fit a low-order polynomial to the spectrum taken on day 207, excluding the Hα region, in order to estimate the continuum flux. We add 50% to this continuum flux and re-normalize the spectrum. The result is plotted in the dashed line in Extended Data Figure 5. This is clearly different than the observed spectrum at day 232, indicating that the increase in bolometric luminosity observed at that day is not due to an increase in the continuum flux alone. This result further disfavors CSM interaction as a source of luminosity for iPTF14hls.

X-Ray Observations We observed the location of iPTF14hls with the X-Ray Telescope (XRT)[57] on-board the *Swift* satellite[58] on 2015 May 23.05. In total 4.9 ks of live exposure time was obtained on the source. We use on-line analysis tools[59, 60] to search for X-ray emission at the location of iPTF14hls. No source is detected with an upper limit on the 0.3–10.0 keV count rate of $< 2.3 \times 10^{-3}\,\mathrm{ct\,s^{-1}}$. Assuming a power-law spectrum with a photon index of $\Gamma = 2$ and a Galactic H column density[61] of $1.4 \times 10^{20}\,\mathrm{cm^{-2}}$, this corresponds to an upper limit on the unabsorbed 0.3–10.0 keV flux of $f_X < 8.4 \times 10^{-14}\,\mathrm{erg\,cm^{-2}\,s^{-1}}$. At the luminosity distance of iPTF14hls this corresponds to a luminosity limit of $L_X < 2.5 \times 10^{41}\,\mathrm{erg\,s^{-1}}$.

Radio Observations Radio emission from SNe may indicate ongoing interaction between the SN ejecta and the CSM (**Assaf: refs**). In search for signs of such interaction we observed iPTF14hls in radio wavelengths using both the Jansky Very Large Array (VLA) and the Arcminute Microkelvin Imager (AMI). The AMI observation was undertaken on 2016 May 18, at 15 GHz and resulted in a null-detection with a 3σ upper limit of $150\,\mu$Jy **Assaf: Two more AMI epochs are reported on marshal**. On 2016 June 10, iPTF14hls was observed with the VLA at 6.1 GHz. The VLA data were reduced using standard CASA software routines where J0920+4441 and 3C286 were used as phase and flux calibrators, respectively. No radio emission was observed at the SN position to a 3σ upper limit of $21.3\,\mu$Jy. **Assaf: some context for this number from interacting SNe - can we limit any CSM parameters?**

Host Galaxy and Redshift Determination We use the SDSS ($ugriz$) and WISE (channels 1 and 2) photometry of the host galaxy (obtained from the respective online databases of both surveys[62, 63]), and fit the 7-band photometry simultaneously with standard SED fitting techniques[64] using the BC03[65] stellar population synthesis models. Due to the blue optical-IR color, only models of low stellar metallicity $< 0.5\,\mathrm{Z}_\odot$ (where $\mathrm{Z}_\odot$ is the solar metallicity) provide a good fit to the data. Assuming a metallicity of $0.2\,\mathrm{Z}_\odot$, the best fit SED is dominated by a population ≈1 Gyr in age with negligible dust extinction ($A_V \lesssim 0.2$ magnitudes) and a star formation rate of $\lesssim 0.4\,\mathrm{M}_\odot\,\mathrm{yr}^{-1}$. The best fit total stellar mass is $3 \pm 1 \times 10^8\,\mathrm{M}_\odot$, similar to that of the Small Magellanic Cloud (SMC), but with a diameter of $\approx 7\,$kpc the iPTF14hls host galaxy is larger than typical low-mass dwarfs. We obtained a spectrum of the host galaxy of iPTF14hls on 2015 Dec 11 with the Low Resolution Imaging Spectrometer (LRIS)[48] mounted on the Keck I 10-meter telescope. We used the $1.0''$ slit centered on the core of the galaxy and rotated to the parallactic angle to minimize the effects of atmospheric dispersion[66] (in addition, LRIS has an atmospheric-dispersion corrector). We used a configuration whereby coverage in the blue with the 600/4000 grism extends over the wavelength range $3200-5600$Å with a dispersion of 0.63Å pixel^{-1} and a full-width at half-maximum intensity (FWHM) resolution of ~ 4Å. We used the 5600Å dichroic, and our coverage in the red with the 400/8500 grating extends over $5600 - 10200$Å with a dispersion of 1.16Å pixel^{-1} and a resolution of FWHM ≈ 7Å. For this observation the region near the dichroic had low flux and was noisy, so we have trimmed it out, leaving a small gap in wavelength coverage. Spectra were reduced using the standard techniques optimized for Keck+LRIS by the `CarPy` package in PyRAF, and flux calibrated to spectrophotometric standard stars obtained on the night of our observations in the same instrument configuration. We determine a redshift of 0.0344 based on narrow host galaxy emission lines of H, S II, O II and O III (Extended Fig. 7; some broad Hα emission from the supernova can also be seen).

Can Time Dilation Explain iPTF14hls? iPTF14hls displays a factor of $\approx 6-10$ slower spectral evolution compared to a normal SN IIP. Relativistic time dilation would cause the spectrum to be redshifted by the same factor of $\approx 6-10$, which is inconsistent with our observed redshift of 0.0344. For a light echo to cause time dilation (in addition to time delay), the reflecting surface would have to be moving away from the light source at a velocity comparable to the speed of light divided by the time dilation factor. The required time dilation then implies an improbably high velocity for the reflecting surface of $\approx 0.1c$ (with c the speed of light). The light echo interpretation is also difficult to reconcile with the observed emission being more luminous than any previously observed IIP SN. We therefore rule out time dilation effects and conclude that the slow spectral evolution of iPTF14hls is intrinsic to the SN.

The Ejecta Mass of iPTF14hls The optical depth τ in a shell of mass M, radius R and opacity κ is $M\kappa/4\pi R^2$ (we assume spherical symmetry, as implied by the shape of the P-Cygni profiles observed in the spectra). The resulting mass needed to maintain an optically thick shell ($\tau = 1$) is then $M \approx 2\mathrm{M}_\odot \kappa_{0.34}^{-1} R_{16}^2$ where $\kappa_{0.34}$ is the opacity in units of $0.34\,\mathrm{cm}^2\,\mathrm{g}^{-1}$ (as appropriate for hydrogen-rich material) and R_{16} is the radius in units of $10^{16}\,\mathrm{cm}$. The measured $v{\cdot}t$ radius of $\approx 2{\cdot}10^{16}\,\mathrm{cm}$ at day 600 from discovery (assuming the expansion started at discovery), with the spectrum still photospheric then, implies an ejecta mass of $\approx 8\,\mathrm{M}_\odot$ which is typical of Type IIP SNe. However, if we set the start date of the expansion to 3500 days earlier, as required by the $v \propto t^{-0.464}$ fit to the velocity evolution, then the implied radius is $\approx 10^{17}\,\mathrm{cm}$ which requires an ejecta mass of $\approx 200\,\mathrm{M}_\odot$.

The Divergent Photospheric Radii of iPTF14hls As explained in the main text, we measured the photospheric radius using two methods and find diverging results. This could be explained if the line-producing photosphere and the continuum-producing photosphere are somehow decoupled. However, such decoupling has never been observed for IIP SNe, nor is it explained by any existing SN model. An alternative explanation to the diverging photospheric radii is that the homologous expansion assumption is invalid, and mass is continuously being injected into the system as a high-velocity outflow from a central source, In such a case, $v{\cdot}t$ no longer represents a radius since t no longer represents the time it takes mass traveling at velocity v to reach the photosphere. However, there is no known mechanism to create continuous mass outflows at SN-ejecta velocities (several thousand $\mathrm{km\,s^{-1}}$) as observed for iPTF14hls (Fig. 3).

Extended Data

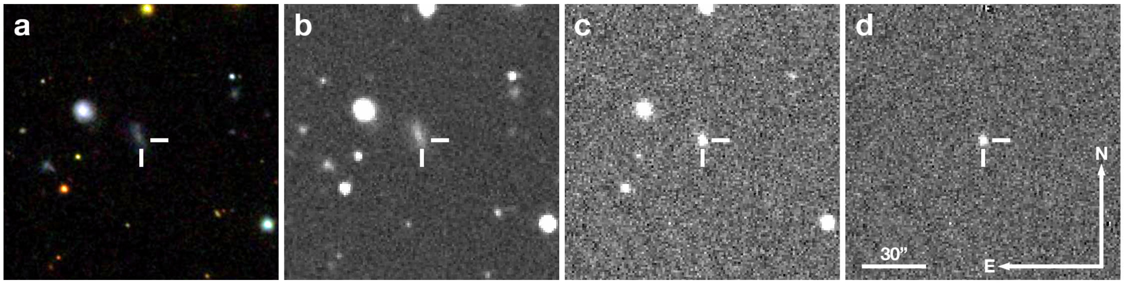

Extended Data Figure 1 SDSS image centered at the position of iPTF14hls (**a**), Palomar 48-inch deep co-added pre-discovery reference image (**b**), Palomar 48-inch discovery image of iPTF14hls (**c**) and the result of subtracting the reference image from the discovery image (**d**). The position of iPTF14hls is indicated by tick marks in each image.

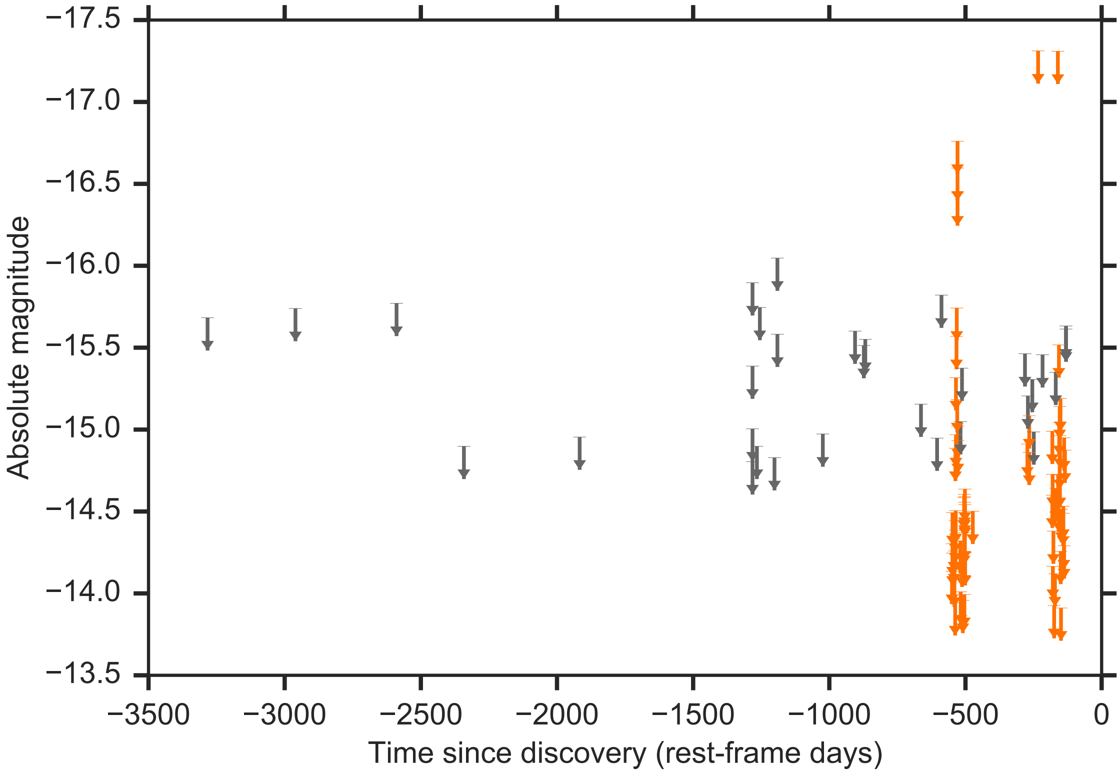

Extended Data Figure 2 Pre-explosion non-detection limits of iPTF14hls from P48 (red arrows, Mould-R band, 3σ non-detections) and from CSS (unfiltered, obtained via the CSS website).

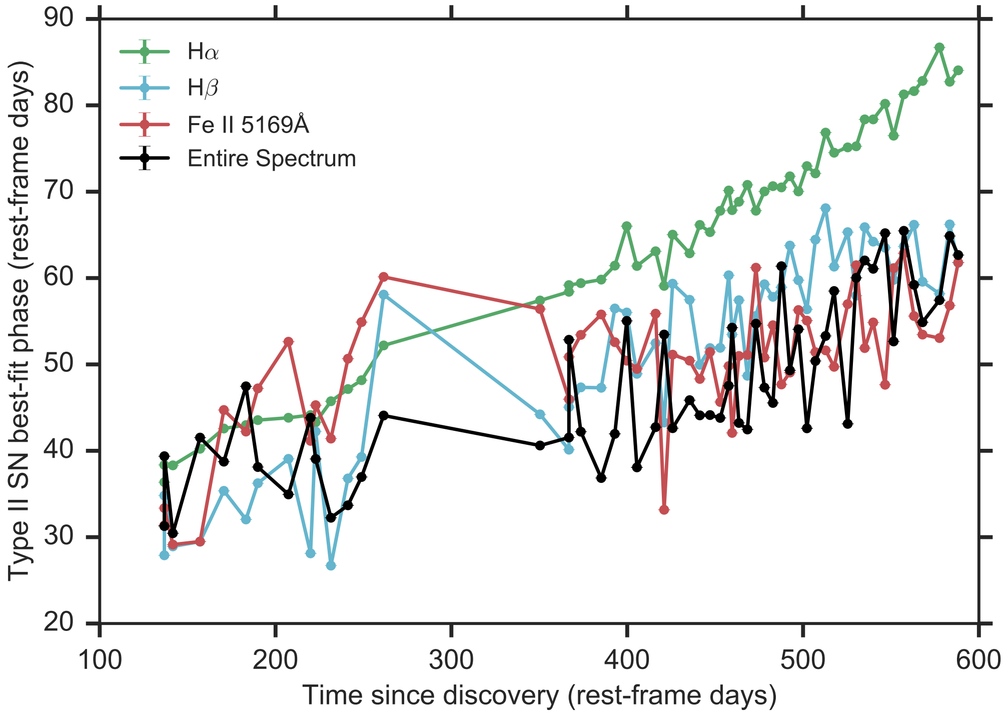

Extended Data Figure 3 Best-fit phase of iPTF14hls spectra from Superfit[53], compared to the true spectral phase, when fitting the entire spectrum (black) or only certain line regions as noted. The spectra of iPTF14hls are similar to those of other Type II SNe but are a factor of 6-10 slower evolving.

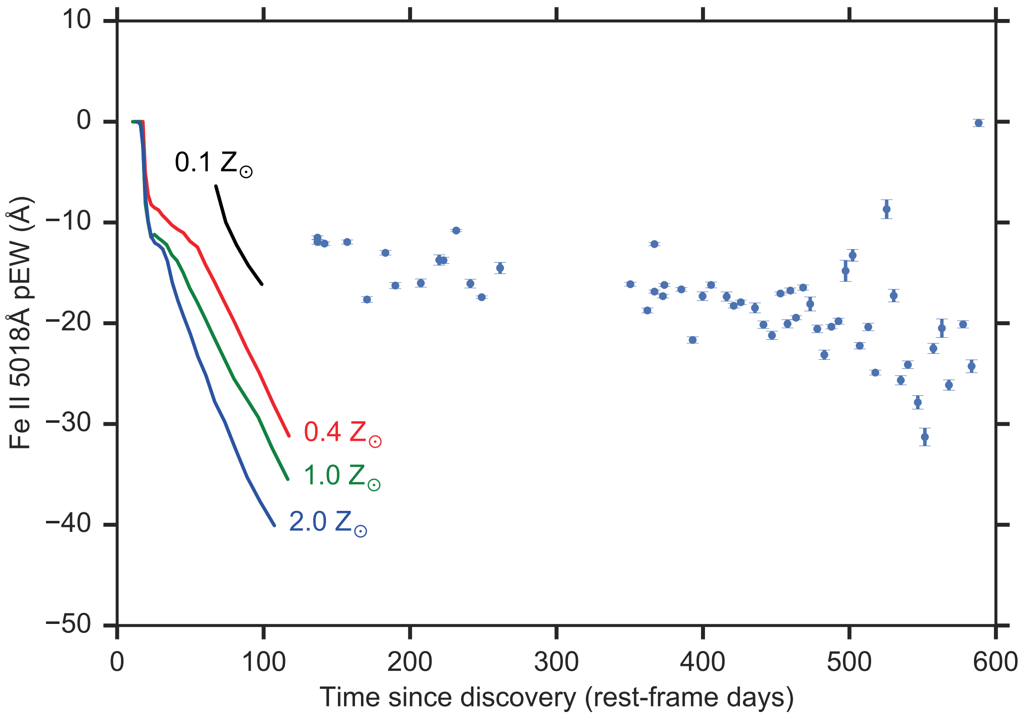

Extended Data Figure 4 Fe II 5018Å absorption pseudo equivalent width (pEW) measurements for iPTF14hls (circles). Values from theoretical models[54] of different progenitor metallicities are also shown (lines; $Z_\odot$ is the solar metallicity). iPTF14hls may have had a low metallicity progenitor, though the models do not extend to late enough times to allow for an accurate comparison.

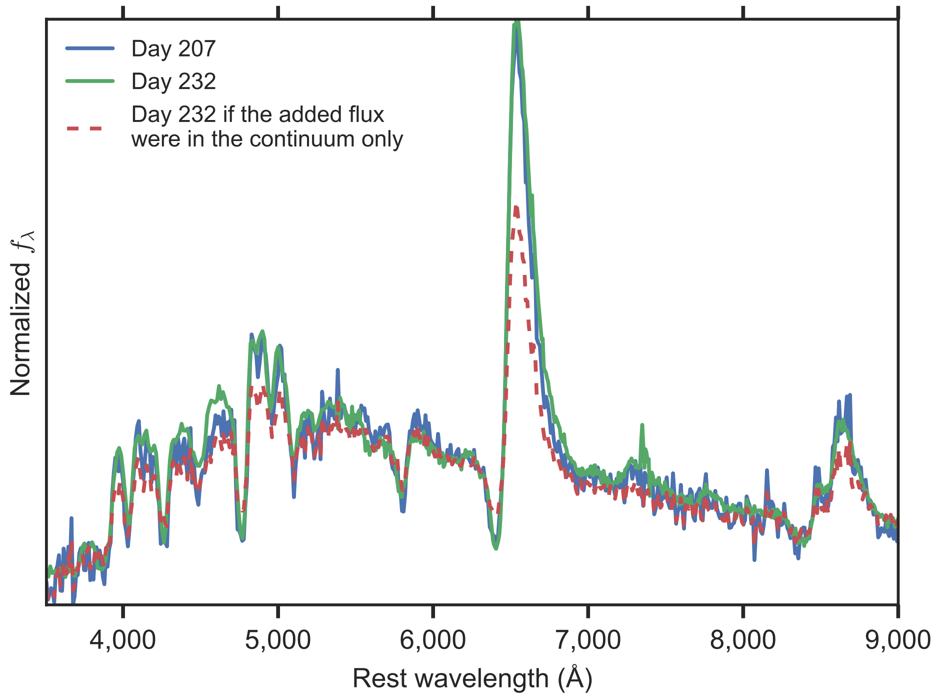

Extended Data Figure 5 Spectra of iPTF14hls expressed in terms of normalized flux density as a function of rest-frame wavelength taken on rest-frame days 207 (right before the rise to the brightest peak in the light curve) and 232 (at the brightest peak in the light curve) after discovery (solid lines). The similarity of the spectra indicate that the increase of $\approx 50\%$ in luminosity observed in the light curve between the two epochs is equal at all wavelengths. If the increase were only to the continuum flux, then the line emission on day 232 would have been diluted in the continuum (as simulated by the dashed line).

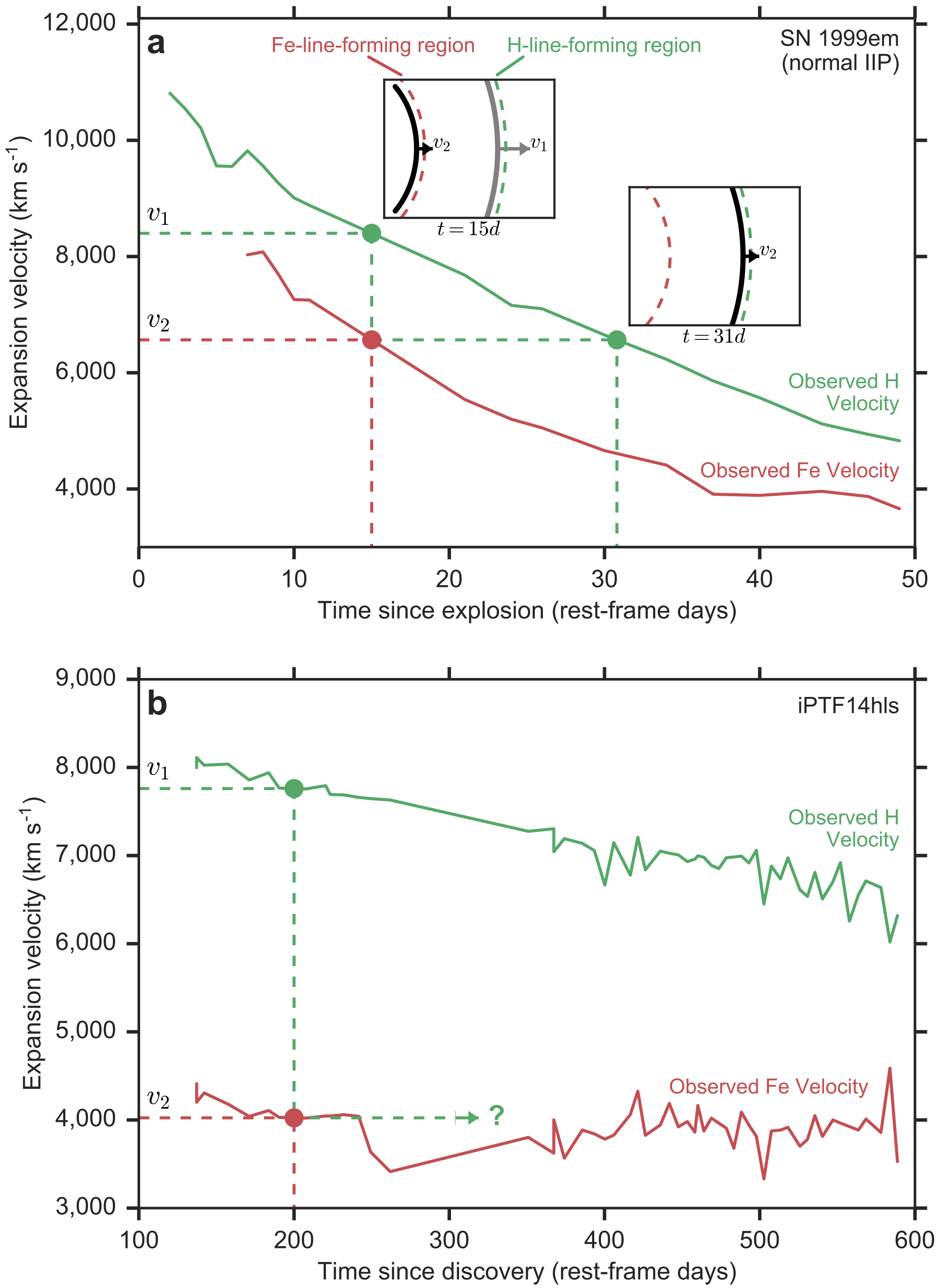

661

662 **Extended Data Figure 6** Evolution of the measured velocity gradient in the normal Type IIP

SN 1999em[34] (**a**) and in iPTF14hls (**b**). At a given time, the H-line-forming region is at material expanding with velocity v_1, while the Fe-line-forming region is at material expanding with lower velocity v_2 (top inset in panel **a**). For SN 1999em, the H-line-forming region soon reaches the material expanding at velocity v_2 as it moves inwards in mass (bottom inset in panel **a**) and v_2 is measured in the H lines. For iPTF14hls, in contrast, the H-line-forming region does reach the material expanding at v_2 even after the time since discovery increases by a factor of 6. If the material were ejected soon before discovery, this would indicate an increase in the radius of the line forming regions by a factor of ≈ 6, which is unlikely given the observed velocity gradient between the H and Fe lines. If the material were ejected long before discovery, on the other hand, the relative expansion in radius would be much smaller. This case is discussed in the main text.

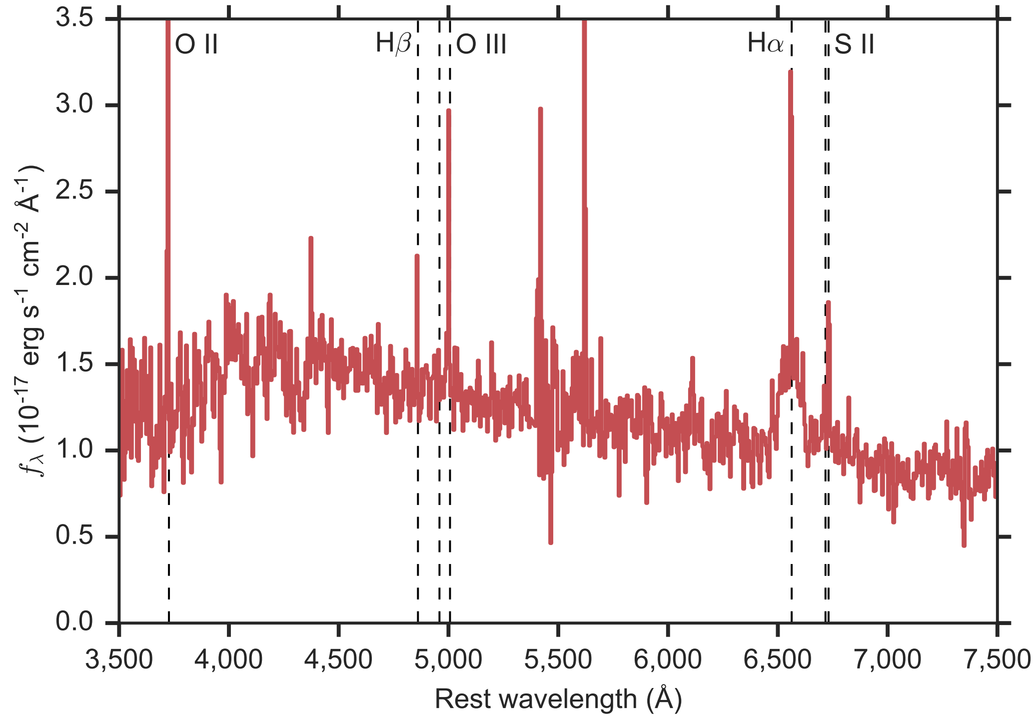

Extended Data Figure 7 Spectrum of the host galaxy of iPTF14hls, expressed in terms of flux density as a function of rest-frame wavelength, obtained by positioning the slit on the center of the host, away from the SN. Some SN contamination is present, precluding the precise measurement of host galaxy line fluxes, but clear narrow emission lines can be seen, indicative of ongoing star formation. The annotated lines allow an accurate redshift determination of $z = 0.0344$. The spectrum has been binned in wavelength for clarity.

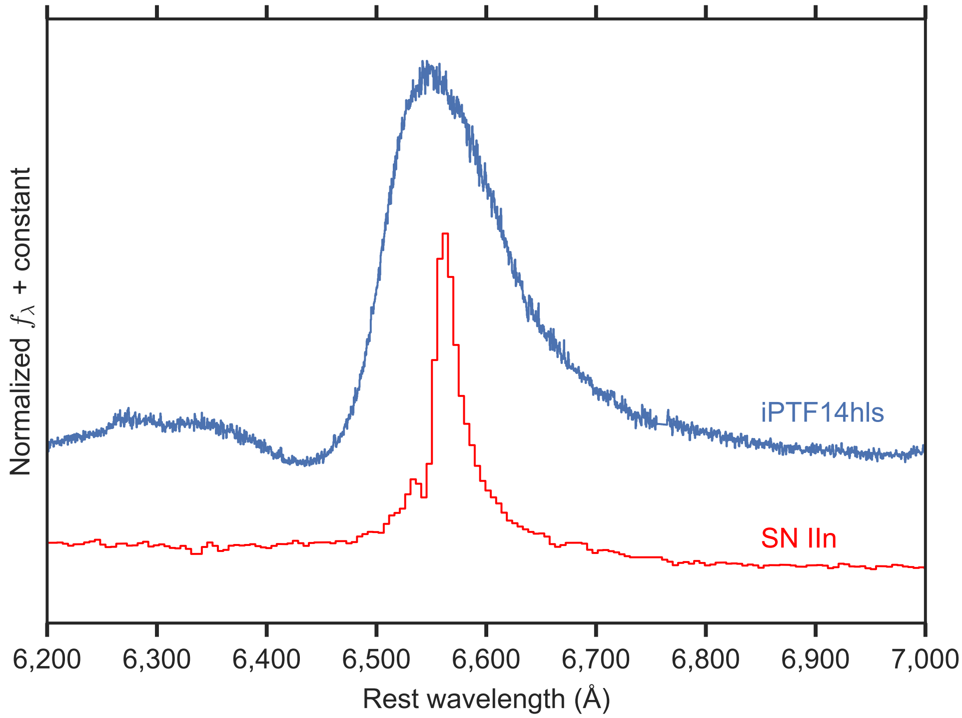

Extended Data Figure 8 The Hα region in our highest resolution spectrum of iPTF14hls taken on 2016 June 4 using DEIMOS on Keck II (blue), expressed in terms of normalized flux density as a function of rest-frame wavelength, compared to the interaction-powered Type IIn SN 2005cl[20] (red). iPTF14hls shows no signs of narrow emission or narrow P-Cygni features as seen in interacting SNe.

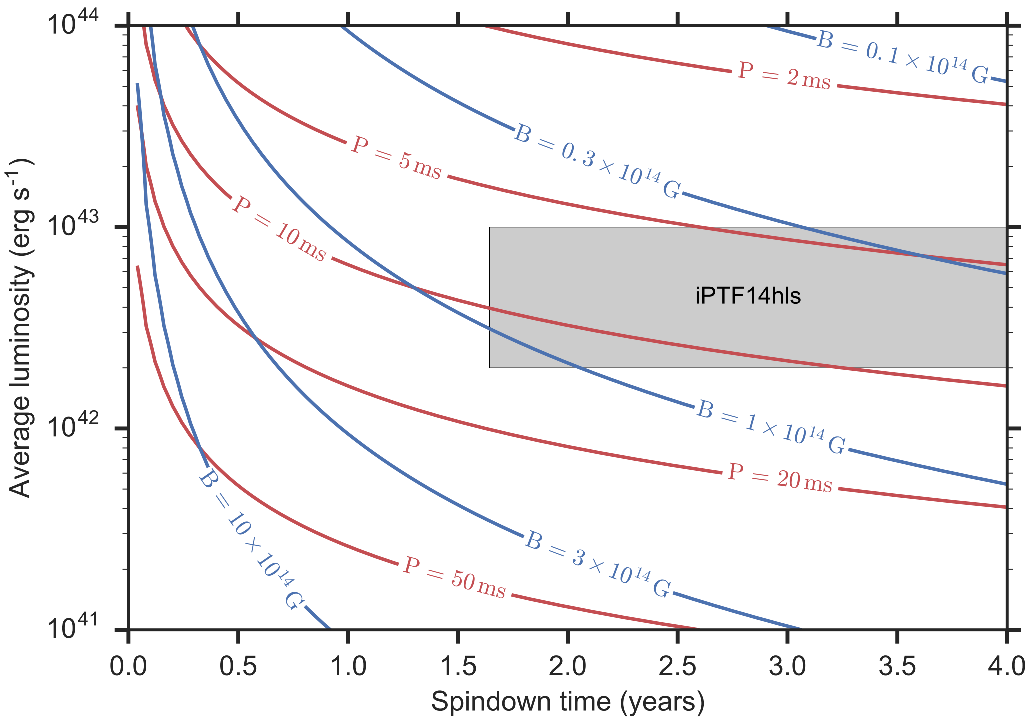

Extended Data Figure 9 Magnetar initial spin period, P (red), and magnetic field, B (blue), required to produce transients of different time scales (x-axis) and average luminosities (y-axis)[5]. The time-scale and average luminosity of iPTF14hls (grey area representing only a lower limit on the time-scale, as the event is still ongoing, assuming it keeps the same average luminosity) can be reproduced by a magnetar with an initial spin period of $\approx 5 - 10\,$ms and a magnetic field of $\approx 0.5 - 1 \times 10^{14}$ Gauss.